Supporting information for:

Amyloid-β peptide interactions with amphiphilic surfactants: electrostatic and hydrophobic effects

Nicklas Österlund[a,b], Yashraj S. Kulkarni[c], Agata D. Misiaszek[c], Cecilia Wallin[a], Dennis M. Krüger[c], Qinghua Liao[c], Farshid Mashayekhy Rad[b], Jüri Jarvet[a,d], Birgit Strodel[e], Sebastian K.T.S. Wärmländer[a], Leopold L. Ilag[b], Shina C.L. Kamerlin[c*], Astrid Gräslund[a*]

[a] Department of Biochemistry and Biophysics, Arrhenius Laboratories, Stockholm University, 106 91 Stockholm, Sweden.

[b] Department of Environmental Science and Analytical Chemistry, Arrhenius Laboratories, Stockholm University, 106 91 Stockholm, Sweden.

[c] Department of Cell and Molecular Biology, Uppsala University, 751 24 Uppsala, Sweden

[d] The National Institute of Chemical Physics and Biophysics, Tallinn, Estonia.

[e] Institute of Complex Systems: Structural Biochemistry, Forschungszentrum Jülich, 52425 Jülich, Germany

Corresponding author email addresses: astrid.graslund@dbb.su.se and kamerlin@icm.uu.se

Table of Contents

Supporting Description of Computational Methodology

All molecular dynamics (MD) simulations performed in this work were based on the solution NMR structure of the Aβ(1-40) peptide in a water-micelle environment (PDB ID: 1BA4)[1,2], in complex with pre-generated micelles using the standard Micelle Maker protocol without post-processing (i.e. no minimization or equilibration in Micelle Maker).[3] Specifically, the third NMR conformer of the structural ensemble was used for the simulations due to the long and straight α-helical conformation observed for residues 15-36. A random coil conformation of the peptide was taken from a 400 ns MD simulation at 300 K starting from the NMR structure for subsequent study. This simulation was done using the exact same protocol that was used for all the other simulations in this study.

The SDS and DDM micelles, with 62 and 98 individual molecules respectively, were generated by Micelle Maker, putting these micelles within the size range provided by experimental studies.[4] The initial Aβ-micelle complexes were then generated manually using PyMOL version 1.7.2.1.[5] Two different Aβ-micelle complexes were tested, with (1) a random coil structure of the peptide on the micellar surface, and (2) an α-helical form of the peptide inserted into the core of the micelle. In the case of the random coil structure, the peptide was manually placed within 5 Å of the micellar surface in the initial structure, allowing the peptide to adjust to the micelle by itself in the initial phases of the simulation. In the case of the other structures where the α-helical part of the peptide was buried inside the micelle, the peptide was manually inserted into the micelle through a gap generated between individual micelle molecules, and bad steric contacts between the peptide and the SDS/DDM molecules inside the micelle were removed using the geometry clean-up tool implemented in Maestro v. 11.1.012 (Release 2017-1). Two different insertion depths of Aβ were considered: one with residues 17–40 fully inserted into the micelle, and another one in which only the C-terminal residues 29–40 were inserted into the core of the micelle. These complexes, which are shown in Figure S10, were used as starting points for subsequent MD simulations. However, for simulations involving the random coil Aβ(1-40) peptide, one initial structure was used with a unique random seed for each independent simulation. As a control experiment, the two different conformations of Aβ(1-40) peptide alone – random coil and α-helical – were also simulated in a water box under identical conditions as all the other simulations.

All MD simulations in this work were performed with the GPU implementation of the AMBER16 software package[6] and all model systems were prepared for simulation using the LEaP module of AmberTools 16. The ff14SB[7] force field implemented in AMBER16 was used for Aβ(1-40), while for the SDS and DDM molecules the GLYCAM_06j[8] library and force field were employed. Asp, Glu, Lys and Arg residues were all kept in their ionized states. The His residues (H6, H13 and H14) were protonated at the epsilon N atom. The N-terminus was positively charged while the C-terminus was negatively charged. Each model system was placed in an octahedral TIP3P water box[9,10], extending at least 11 Å from the solutes in each direction. All systems were neutralized by addition of Na^+ or Cl^- counter ions as applicable depending on the total charge of the peptide-micelle complex, and additional counter ions were then added to the system to maintain a standard ionic strength of 0.15 M in the water box. Each ion was added by randomly replacing an existing water molecule in the solvent box, using "addions" of the LEaP module. The solvated systems were then subjected to a two-step minimization procedure in order to remove clashes between the water molecules and the solute. This was comprised of (1) 50 steps of steepest descent and 200 steps of conjugate gradient minimization using 25 kcal mol^{-1} $Å^{-2}$ harmonic positional restraints on all solute atoms, followed by (2) 50 steps of steepest descent and 200 steps of conjugate gradient minimization with weaker 5 kcal mol^{-1} $Å^{-2}$ harmonic positional restraints on all solute atoms. After this initial minimization, four sequential equilibration steps were performed: (1) a 50-ps NVT simulation to increase the thermostat target temperature from 100 K to 300 K using the Berendsen thermostat[11] with 0.5 ps time constant for the bath coupling; (2) a 50-ps NPT simulation at a constant isotropic pressure of 1 atm and a constant temperature of 300 K to adjust the density of the system to 1 g cm^{-3} using the Berendsen barostat and thermostat; (3) five 50-ps NVT simulations in which the remaining 5 kcal mol^{-1} $Å^{-2}$ harmonic positional restraints were progressively decreased in 1 kcal mol^{-1} $Å^{-2}$ increments, allowing us to finally perform (4) a 50-ps NVT simulation without any restraints on the system.

For the production runs, we performed for each system three independent simulations using a different initial configuration of the Aβ(1-40) micelle complex. All simulations were performed using a 2 fs time step, saving snapshots every 20 ps. The SHAKE algorithm[12] was used during the dynamics to constrain all bonds involving hydrogen atoms. The van der Waals interactions were calculated with a cut-off of 8.0 Å, while the electrostatic interactions were treated with the particle mesh Ewald (PME) method[13] with a cut-off of 8 Å. The temperature was kept constant at 300K using Berendsen's weak coupling algorithm.[12] All

production simulations were performed using NVT conditions. Three replicas of 1 μs length each system were performed, leading to a simulation time of 3 μs per system and 24 μs in total (see Table S2).

Supporting Figures

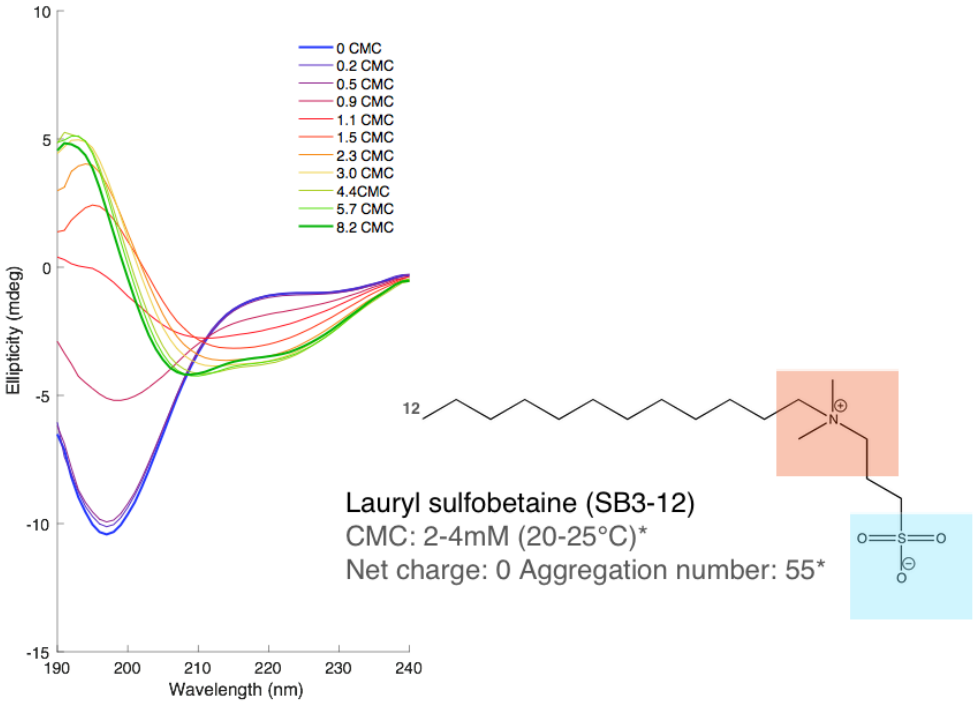

Figure S1. CD spectra of 40 μM Aβ (1-40) in 10 mM sodium phosphate buffer pH 7.3 at increasing concentrations of SB3-12. SB3-12 has a shorter hydrophobic tail than SB3-14 (12 carbon atoms in contrast to 14 for SB3-14) and a 10 times higher CMC. The CD spectra are almost identical to that obtained after addition of SB3-14 to the peptide (Figure 1B), with β-sheet structures formed above the CMC and α-helical structures formed when the number of micelles are larger than the number of peptides. * Values from Sigma Aldrich.

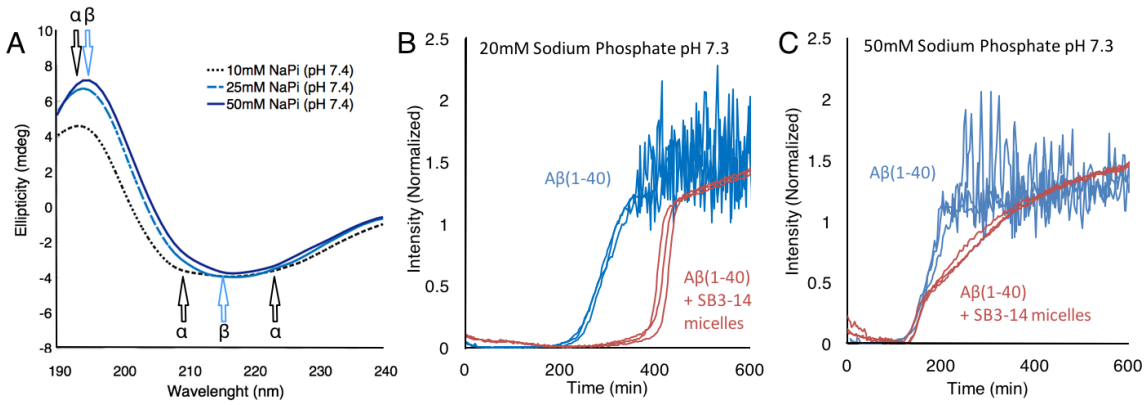

Figure S2. Effect of ionic strength on the Aβ/SB3-14 micelle interaction as seen by: CD spectroscopy (A), arrows indicate wavelengths reporting on α-helical and antiparallel β-sheet secondary structure. ThT fluorescence at 20 mM (B) sodium phosphate buffer and 50mM (C), blue trace shows the peptide without any surfactant and the red trace shows the peptide in presence of SB3-14 micelles. **20** μM Aβ at 37 °C under quiescent conditions.

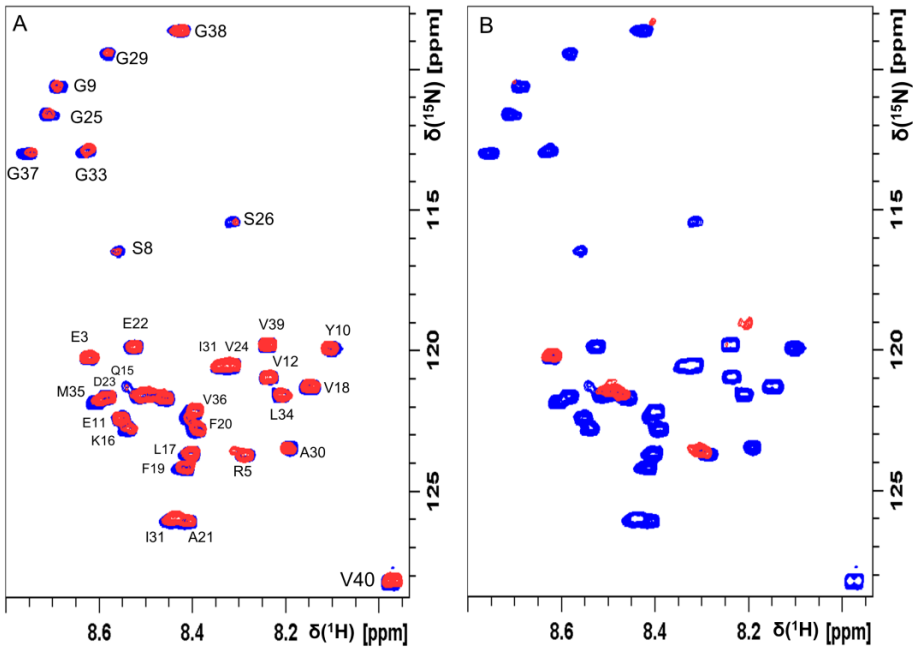

Figure S3. Blue crosspeaks: 2D NMR 1H-15N-HSQC spectra of 84 μM 15N-labeled Aβ(1-40) Red crosspeaks: ^{1}H-^{15}N-HSQC spectra of 84 μM ^{15}N-labeled Aβ(1-40) upon addition of A) 0.7 mM and B) 2.0 mM SB3-14 surfactant. Spectra recorded with a 500 MHZ Bruker Avance spectrometer with a cryoprobe at 288 K.

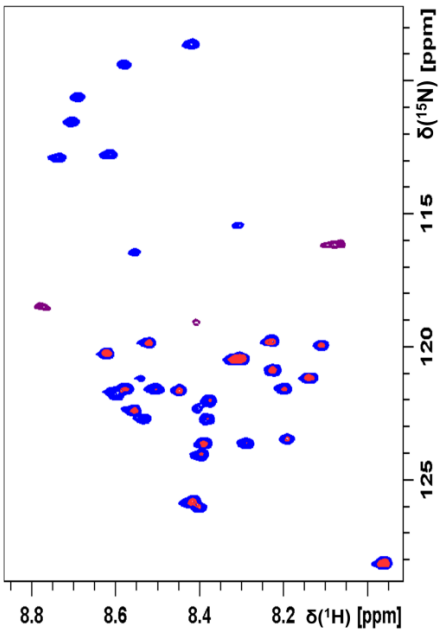

Figure S4. ^{1}H-^{15}N-HSQC spectra of 84 µM ^{15}N-labeled Aβ(1-40) peptides (blue), 84 µM ^{15}N-labeled Aβ(1-40) upon addition of 0.1 mM CTAB surfactant (red) and 84 µM ^{15}N-labeled Aβ(1-40) upon addition of 2.1 mM CTAB surfactant (purple). Spectra recorded with a 700 MHZ Bruker Avance spectrometer with a cryoprobe at 288 K.

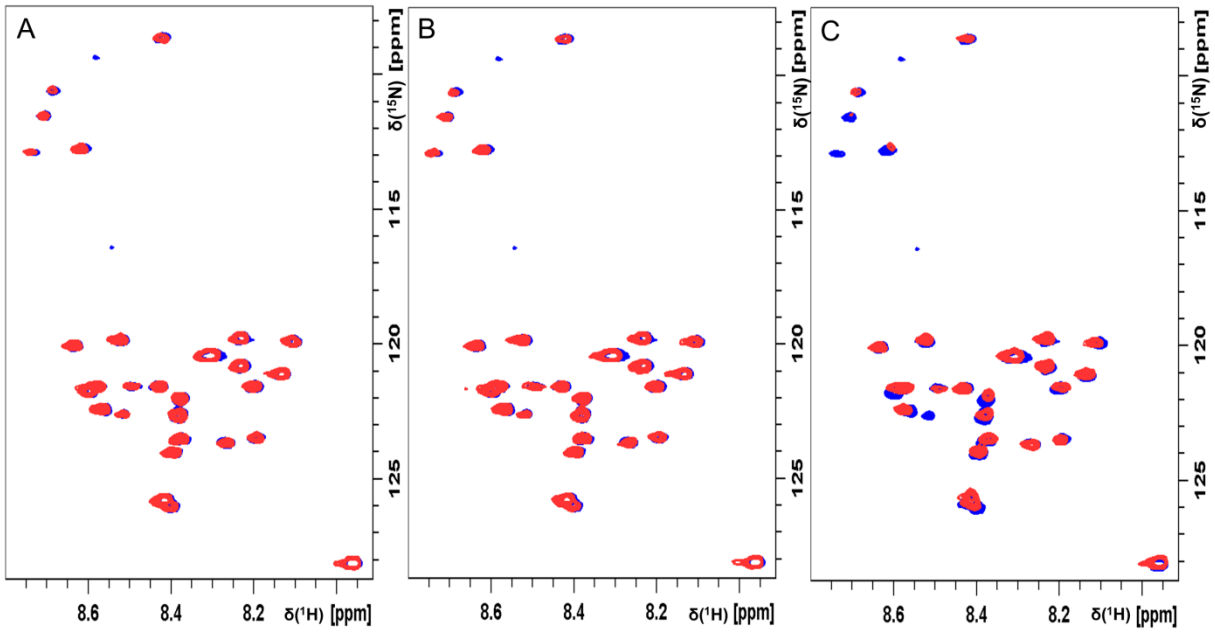

Figure S5. Blue: ^{1}H-^{15}N-HSQC spectra of 84 µM ^{15}N-labeled Aβ(1-40) **Red:** ^{1}H-^{15}N-HSQC spectra of 84 µM ^{15}N–labelled Aβ(1-40) upon addition of 0.05 mM (A), 0.3 mM (B), 3 mM (C) DDM surfactant. Spectra recorded with a 700 MHZ Bruker Avance spectrometer with a cryoprobe at 288 K.

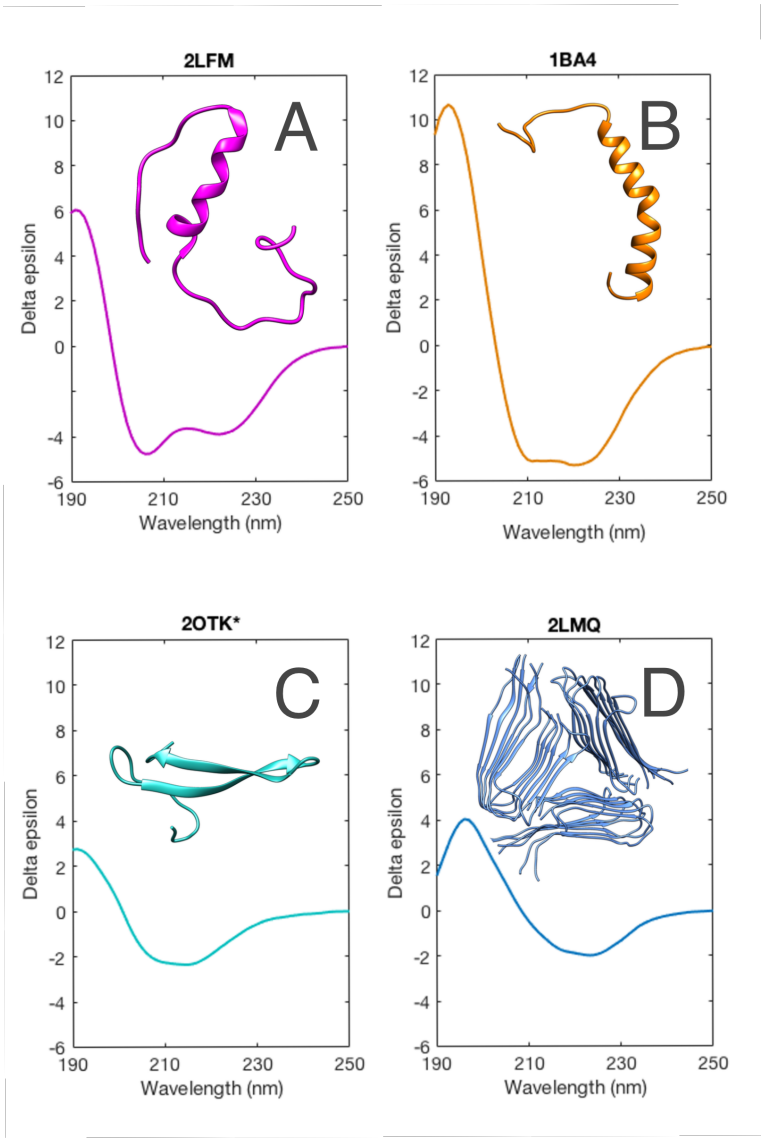

Figure S6. Theoretical CD spectra generated using the pdb2cd software, for some Aβ structures deposited in the pdb. A-B: coil/helix structures from solution (A) and SDS micelle (B). C-D: β-sheet structures of the monomer in a hairpin state determined from an affibody complex (C) and an amyloid fibril (D). *20TK structure was modified by removing affibody atoms and adding an unstructured N-terminal part corresponding to residues 1-15 which are missing from the original NMR structure.

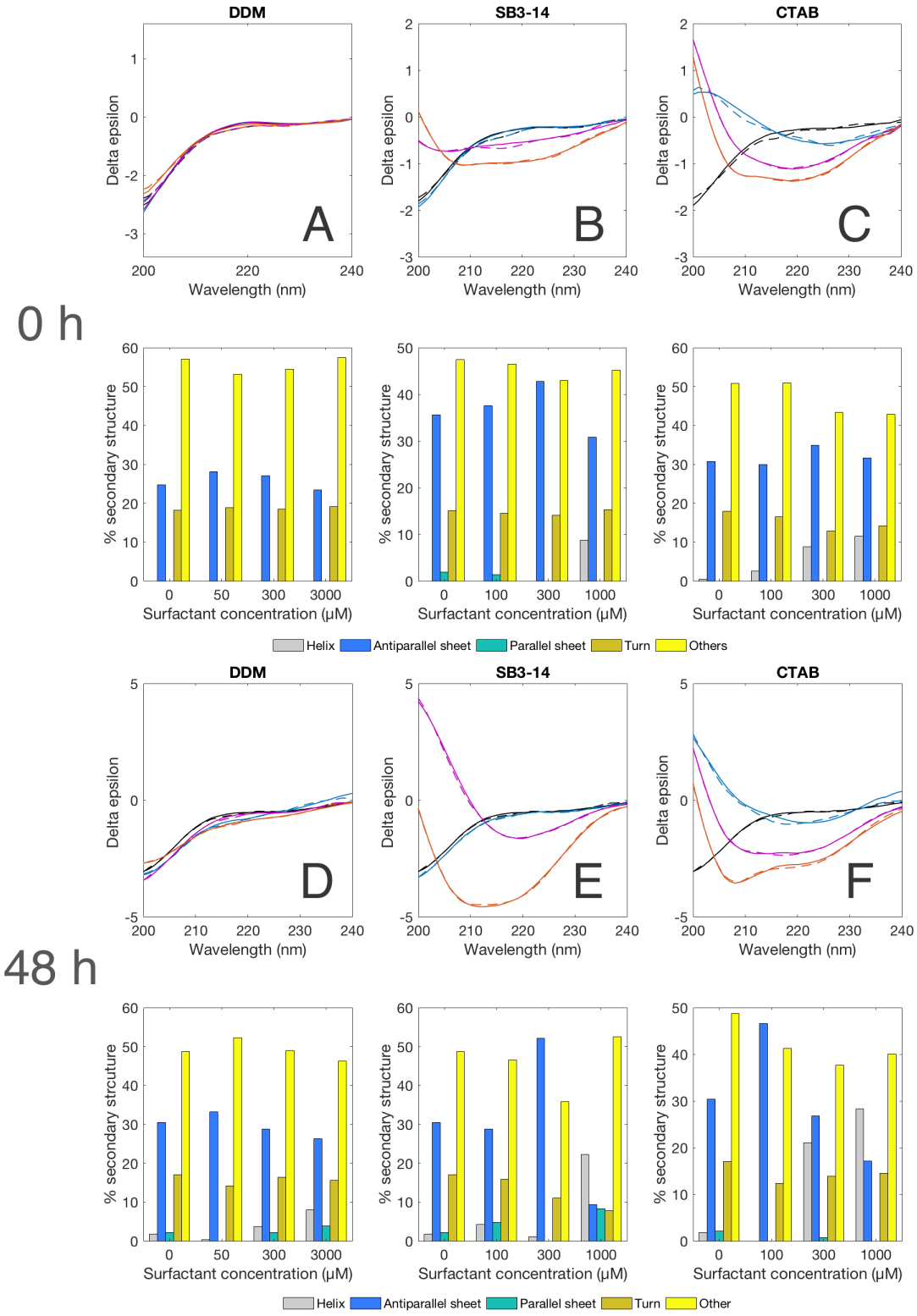

Figure S7. Deconvolution of circular dichroism spectra of 10 μM Aβ(1-40) before (black trace) and after addition of surfactants at one concentration below the CMC (blue) and two concentrations above the CMC (purple, red) at t = 0 h (A-C) and at t = 48 h at 37 °C (D-A). Top panel show the experimental data (solid line) and the theoretical spectrum fitted by the model (dashed) while the bottom panel show the amount of secondary structure determined by the model.

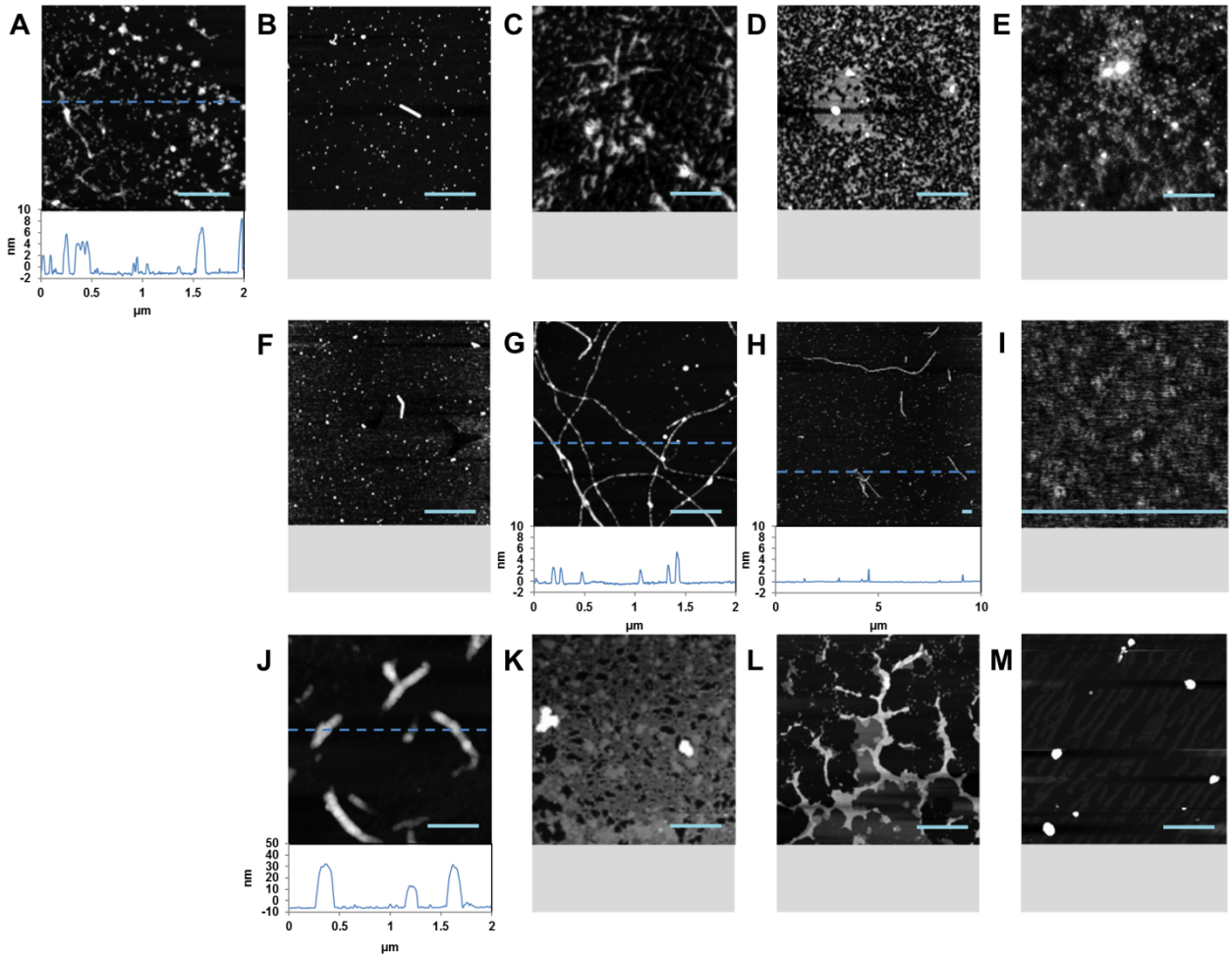

Figure S8. Solid-state AFM images of Aβ(1-40) in the presence and absence of the surfactants DDM, SB3-14, and CTAB. (A) Aβ control in buffer. (B) Aβ and 50 µM DDM. (C) Aβ and 300 µM DDM. (D) Aβ and 3000 µM DDM. (E) 3000 µM DDM control. (F) Aβ and 100 µM SB3-14. (G) Aβ and 300 µM SB3-14. (H) Aβ and 1000 µM SB3-14. (I) 1000 µM SB3-14 control. (J) Aβ and 100 µM CTAB. (K) Aβ and 300 µM CTAB. (L) Aβ and 1000 µM CTAB. (M) 1000 µM CTAB control. The images were recorded with 10 µM Aβ(1-40) samples collected after 48 hours of incubation at +37 °C without agitation (same samples as in the CD measurements in Figure S7). Under these conditions Aβ alone in buffer does not form any typical amyloid fibrils, which was confirmed with a mainly disordered random coil structured CD spectrum (black traces in Figure S7. D-F). The images corresponding to Aβ in the presence of 300 µM SB3-14 (G), 1000 µM SB3-14 (H), or 100 µM CTAB (J), all show clear fibrillar structures. The presence of fibrils under these conditions is in agreement with the secondary structure determinations displaying β-sheet structures in the respective CD spectra (Figure S7. E and F), and with increased ThT fluorescence intensity over time (Figure 4C in the main manuscript). In the presence of DDM, low concentration of SB3-14, or with CTAB concentrations above CMC, no typical amyloid fibrils were observed. Scale bar equals to 0.5 µm.

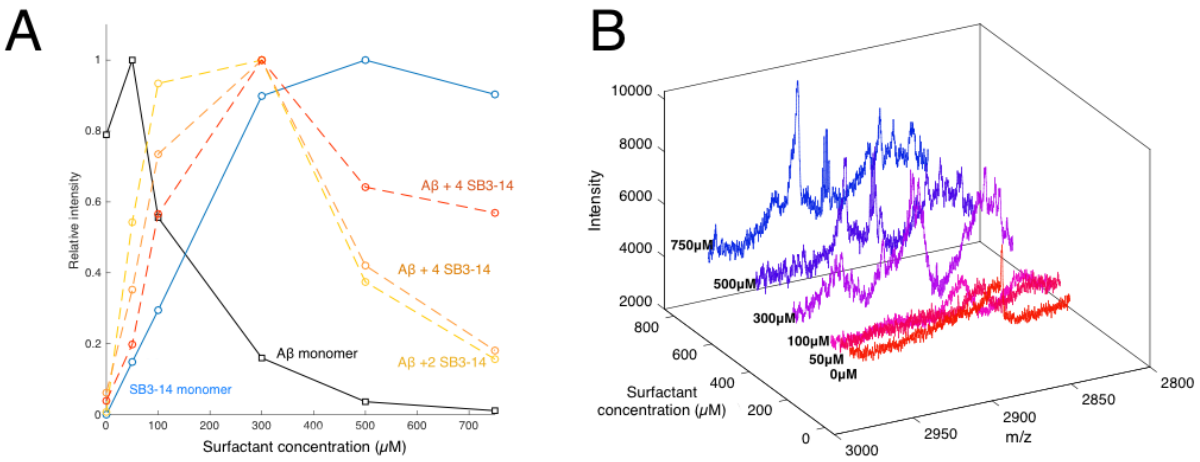

Figure S9. A) Mass spectrometry data show an initial increase of monomeric peptide followed by a rapid decrease upon surfactant titration additions. Instead, peptide-surfactant clusters are formed until reaching a surfactant concentration of 300 μM. The gas phase CMC seems to agree with solution state CMC. B) Above the CMC value given in Figure S6A, large and broad peaks appear in the higher m/z range. Shown is a representative section. The broad nature of the peaks makes charge state deconvolution and therefor direct identification of the peaks not possible.

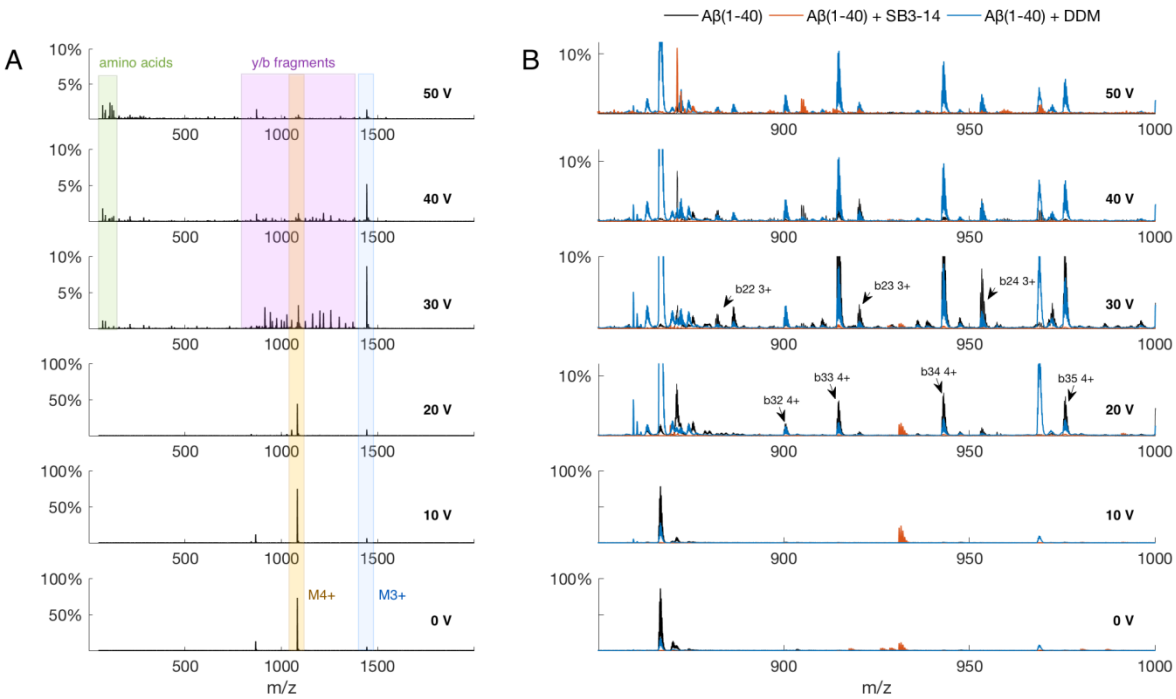

Figure S10. Peptide fragmentation upon increased collisional voltage. A) The Aβ(1-40) peptide without surfactant at increasing collisional voltage. B) A representative region for b-ion fragments (m/z 800-1000), for Aβ(1-40) without surfactant (black), and upon addition of SB3-14 micelles (red) and DDM micelles (blue).

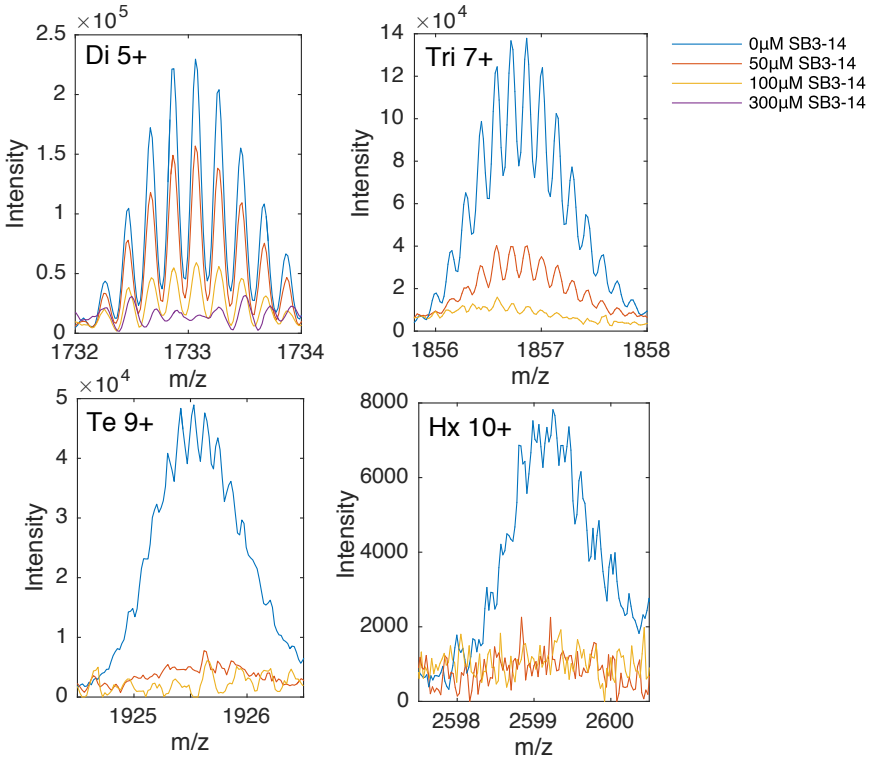

Figure S11. Mass spectra of Aβ (1-40) oligomers at different surfactant concentrations. Addition of surfactant dissolves oligomers; larger oligomers are more affected than smaller ones. Di = dimer, Tri = trimer, Te = tetramer, Hx = hexamer. Number indicates the charge state of the oligomeric assembly.

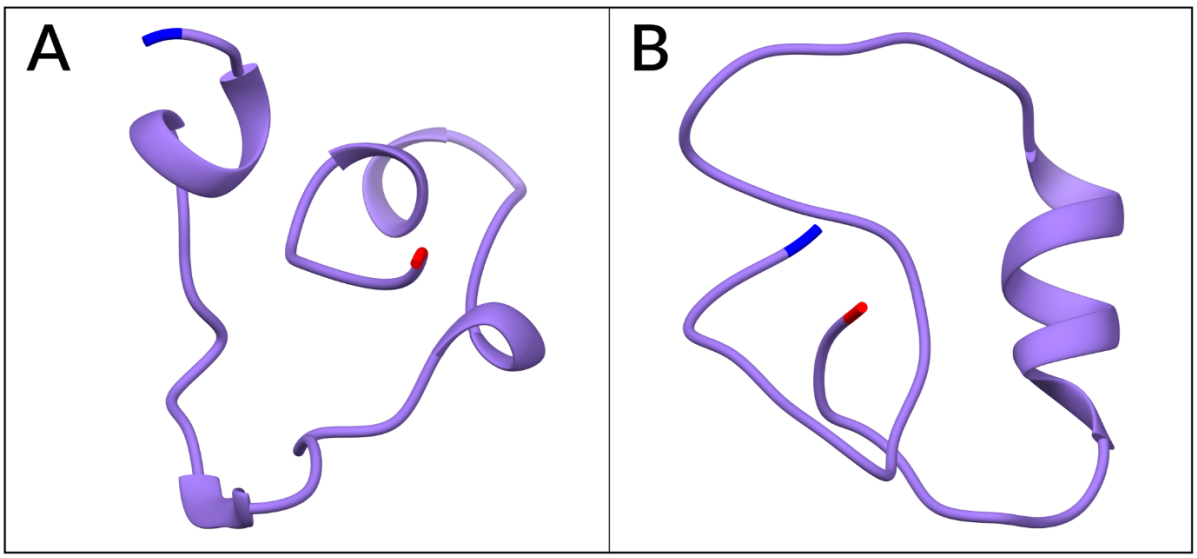

Figure S12. Top ranked cluster representations from "control" MD simulations of A) a random coil Aβ(1-40) peptide in water, and B) an α-helical Aβ(1-40) peptide in water. The Aβ-peptide is shown in purple ribbon representation. The N-terminal residue (D1) is coloured in blue, whereas the C-terminal residue (V40) is coloured in red.

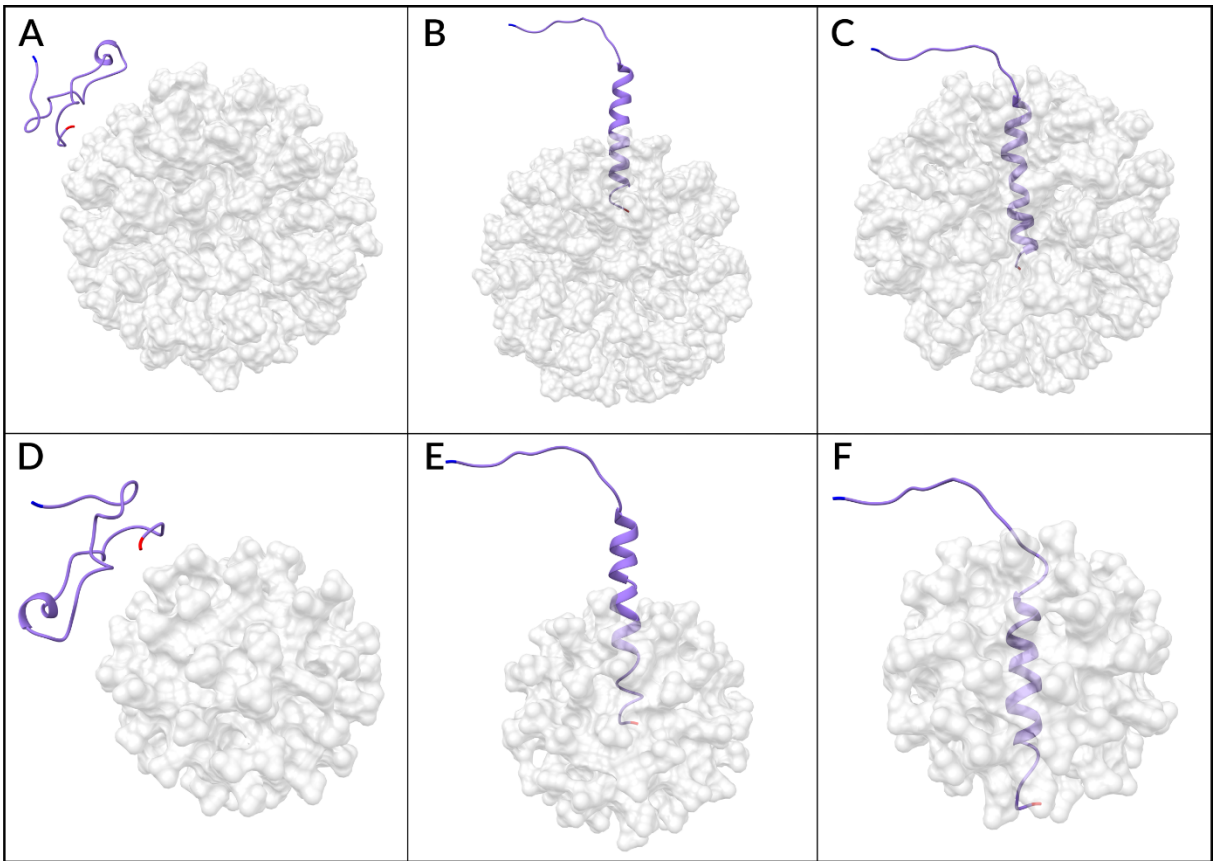

Figure S13. Initial structures of various complexes of Aβ(1-40) with DDM (panels A-C) and SDS (panels D-F) micelles. Panels A and D show the starting structures for random coil Aβ(1-40) placed above the micelle surface. Panels B, C, E and F represent the starting structures for α-helical Aβ(1-40) inserted into the core of the micelle. Of these, B and E are structures where only the hydrophobic C-terminal α-helix (residues 29-40) was inserted into the micelle, whereas C and F are structures with the entire α-helical region (residues 16-40) buried into the micelle. The Aβ peptide is shown in purple ribbon representation. The micelle is shown in grey surface representation. The N-terminal residue (D1) is coloured in blue, whereas the C-terminal residue (V40) is coloured in red. The structures shown in panels B, C, E and F are optimized by the removal of bad steric contacts between the peptide and the micelle using the geometry clean-up tool implemented in Maestro v. 11.1.012 (Release 2017-1).

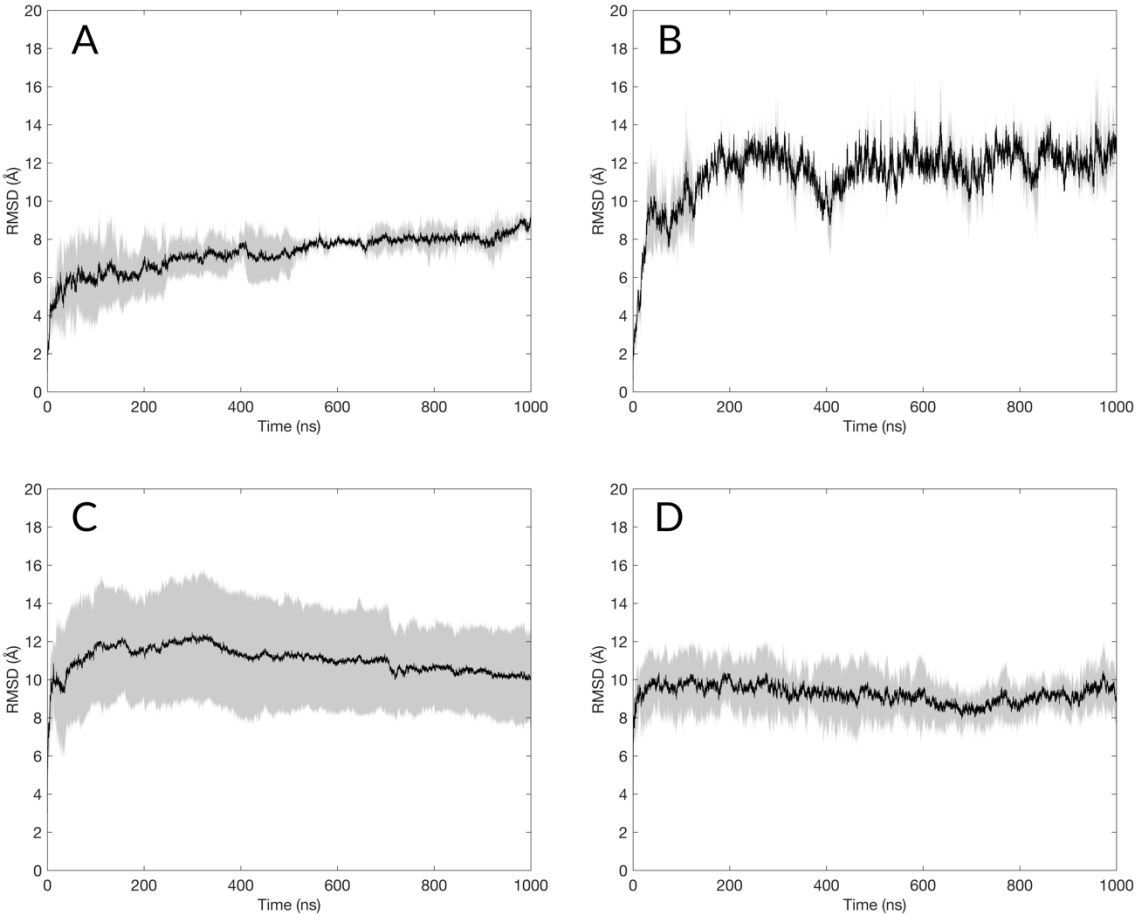

Figure S14. Average RMSD plots from MD simulations of (A) disordered Aβ(1-40) in complex with DDM, (B) disordered Aβ(1-40) in complex with SDS, (C) α-helical Aβ(1-40) in complex with DDM, and (D) α-helical Aβ(1-40) in complex with SDS. For (A) and (B), three individual replicates are averaged whereas for (C) and (D), six replicates are averaged. The RMSD averages are shown in black and the standard deviation is shown in gray. In panels (A) and (B), the peptide was initially placed at a small distance from the micellar surface. In panels (C) and (D), the α-helical part of the peptide was initially inserted into the core of the micelle. The disordered form of the peptide is seen to have a lower RMSD in DDM compared to SDS. On the other hand, the α-helical form of the peptide shows smaller deviation across replicates in SDS whereas the deviations are large in DDM, indicating that this conformation of Aβ(1-40) shows more stable binding in complex with SDS than with DDM.

Supporting Tables

Table S1. Theoretical CMC for the detergents obtained from Sigma-Aldrich as well as experimentally obtained values for hydrophobic clustering from pyrene fluorescence giving a rough estimate of CMC without addition of Aβ(1-40) and upon addition of Aβ(1-40). *Values obtained from Sigma Aldrich.

	DDM (mM)	**SB3-14** (mM)	**CTAB** (mM)
*Theoretical CMC**	0.15	0.1-0.4	0.92-1.0
Experimental CMC (pyrene fluorescence)	0.04	0.09	0.17
Experimental CMC Upon addition of Aβ (pyrene fluorescence)	0.04	0.05	0.02

Table S2. Overview of different simulations performed in this work, and the associated simulation time, to a total of 24 μs of simulation time. All simulations for each system were carried out as three independent 1 μs simulations at 300K and amino acid protonation states mimicking neutral pH (pH = 7).

System	Simulation time (μs)
Random coil Aβ(1-40) in water	3 x 1.0
α-helical Aβ(1-40) in water	3 x 1.0
Random coil Aβ(1-40) on the DDM micelle	3 x 1.0
Random coil Aβ(1-40) on the SDS micelle	3 x 1.0
α-helical Aβ(1-40) buried into the DDM micelle[a]	6 x 1.0
α-helical Aβ(1-40) buried into the SDS micelle[a]	6 x 1.0

[a] These simulations include two configurations of the Aβ(1-40)-micelle complex – one with residues 29-40 inserted into the core of the micelle, and the other with residues 17-40 inserted into the core of the micelle

Table S3. Collisional cross-section values ($Å^2$) of the Aβ(1-40) peptide approximated from the MD simulations using IMPACT[14]. Values are averages over all simulations involving the random coil form of the peptide. The "control" system refers to Aβ(1-40) in water, whereas for the micelle-bound systems, the peptide is bound to the surface of the micelle. Results obtained using the trajectory method (CCS_TJM) are shown.

System	CCS ($Å^2$)
Control	810.95 ± 66.84
Aβ(1-40)-DDM micelle	835.28 ± 53.38
Aβ(1-40)-SDS micelle	960.81 ± 54.35

Table S4. Percentage composition of various secondary structure elements averaged over all the simulations for a particular system. For simulations using unstructured Aβ(1-40) as the initial structure, the averages are taken over three independent 1μs long simulations for the control (peptide in water), Aβ(1-40) with DDM micelle, and Aβ(1-40) with SDS micelle systems. For simulations using α-helical Aβ(1-40) as the initial structure, the averages are taken over three independent 1μs-long simulations for the control (peptide in water), and six independent 1μs long simulations for the Aβ(1-40) with DDM micelle, and Aβ(1-40) with SDS micelle systems. [a] Values belonging to "Initial Structure" are calculated for the random coil, and α-helical conformation of Aβ(1-40) before performing simulations. The secondary structure contents were determined using the STRIDE algorithm.[15]

	Random coil peptide on surface (%)				**α-helical peptide inserted (%)**			
	Initial structure[a]	Control	DDM	SDS	Initial structure[a]	Control	DDM	SDS
α-helix	10.0	11.1	4.5	7.4	57.5	24.3	36.4	42.8
3-10 helix	0.0	8.0	6.4	16.6	0.0	4.1	5.0	4.1
π-helix	0.0	0.0	0.0	0.0	0.0	0.0	0.0	0.1
Strand	0.0	0.4	2.8	0.0	0.0	1.3	0.1	0.0
Turn	67.5	49.4	58.2	50.6	15.0	39.1	28.9	26.6
Coil	22.5	33.0	28.0	25.4	27.5	31.3	29.6	26.4

References

(1) Shao, H.; Jao, S.; Ma, K.; Zagorski, M. G. *J. Mol. Biol.* **1999**, *285* (2), 755–773.

(2) Berman, H. M. *Nucleic Acids Res.* **2000**, *28* (1), 235–242.

(3) Krüger, D. M.; Kamerlin, S. C. L. *ACS Omega* **2017**, *2* (8), 4524–4530.

(4) Clarke, S. *J. Chem. Educ.* **1981**, *58* (8), A246.

(5) Schrodinger LLC. 2015.

(6) D.A. Case, R.M. Betz, W. Botello-Smith, D.S. Cerutti, T.E. Cheatham, III, T.A. Darden, R.E. Duke, T.J. Giese, H. Gohlke, A.W. Goetz, N. Homeyer, S. Izadi, P. Janowski, J. Kaus, A. Kovalenko, T.S. Lee, S. LeGrand, P. Li, C. Lin, T. Luchko, R. Luo, B. Madej, D. M. Y. and P. A. K. M. Y.; Kollman, P. A. *University of California, San Francisco*. 2016.

(7) Maier, J. A.; Martinez, C.; Kasavajhala, K.; Wickstrom, L.; Hauser, K. E.; Simmerling, C. *J. Chem. Theory Comput.* **2015**, *11* (8), 3696–3713.

(8) Kirschner, K. N.; Yongye, A. B.; Tschampel, S. M.; González-Outeiriño, J.; Daniels, C. R.; Foley, B. L.; Woods, R. J. *J. Comput. Chem.* **2008**, *29* (4), 622–655.

(9) Jorgensen, W. L.; Chandrasekhar, J.; Madura, J. D.; Impey, R. W.; Klein, M. L. *J. Chem. Phys.* **1983**, *79* (2), 926–935.

(10) Wu, Y.; Wagner, L. K.; Aluru, N. R. *J. Chem. Phys.* **2016**, *144* (16), 164118.

(11) Berendsen, H. J. C.; Postma, J. P. M.; van Gunsteren, W. F.; DiNola, A.; Haak, J. R. *J. Chem. Phys.* **1984**, *81* (8), 3684–3690.

(12) Ryckaert, J. P.; Ciccotti, G.; Berendsen, H. J. C. *J. Comput. Phys.* **1977**, *23*, 327–341.

(13) Darden, T.; York, D.; Pedersen, L. *J. Chem. Phys.* **1993**, *98* (12), 10089–10092.

(14) Marklund, E. G.; Degiacomi, M. T.; Robinson, C. V.; Baldwin, A. J.; Benesch, J. L. P. *Structure* **2015**, *23* (4), 791–799.

(15) Frishman, D.; Argos, P. *Proteins Struct. Funct. Genet.* **1995**, *23* (4), 566–579.